

Synthesis and characterization of $\text{LiCo}_{1-x}\text{Ni}_x\text{O}_2$ nanoparticles by urea route as cathode for lithium-ion battery

H. T. Homad^{a,b}, N. M. Ali^{a,b}, O. A. Al-Jubouri^b, M. H. Al-Timimi^{*a}

^a*Department of Physics, College of Science, Diyala University, Iraq*

^b*Directorate General of Education in Diyala, Iraq*

$\text{LiCo}_{1-x}\text{Ni}_x\text{O}_2$ ($x = 0, 0.25, 0.5, 0.75, 1$) powders are synthesized using the urea; the crystalline structure and surface morphology of the prepared powders are investigated through XRD, FTIR, FE-SEM, and EDX analyses. X-ray diffraction indicates a hexagonal crystal structure for the LiCoO_2 phase. Additionally, the XRD pattern of prepared LiCoO_2 doped with Ni metal ($x = 0.25$) shows the formation of a cubic LiCoO_2 nanostructure. FTIR spectra analysis of LiCoO_2 and $\text{LiCo}_{1-x}\text{Ni}_x\text{O}_2$ revealed several vibrational modes, such as (C=O and O-H). FESEM results indicate that all samples have nanostructure dimensions. An EDX spectrum reveals the presence of transition metals (Co) in LiCoO_2 , transition metals (Co and Ni) in $\text{LiCo}_{1-x}\text{Ni}_x\text{O}_2$, and transition metals (Ni) in LiNiO_2 .

(Received October 18, 2023; Accepted December 14, 2023)

Keywords: Urea route, $\text{LiCo}_{1-x}\text{Ni}_x\text{O}_2$, Crystalline structure, Surface morphology, FTIR.

1. Introduction

Development of rechargeable power sources is essential for the progress of electronic devices and biomedical instruments like pacemakers. Portable power technology is crucial in their usage. Researchers concentrate on high energy density sources [1,2]. Numerous battery chemistries like nickel cadmium (Ni-Cd) and nickel metal hydride (Ni-MH) are available, but lithium-ion batteries (Li-ion) are the most popular as they possess significant benefits in energy density [3,4]. The design process for portable electronic devices requires careful consideration in selecting the ideal battery system, which is the primary source of power. Choosing the appropriate battery chemistry and charge management control circuitry is pivotal to any unique application. One crucial aspect of this choice is the battery life, which ultimately impacts the competitiveness of the portable device in the market. Sophisticated battery technology and reduced system power consumption can extend battery life and provide a competitive edge. [5-8]. In order to ensure good quality, it's important to maintain reliability, safety, ease of installation, and low cost from a production standpoint. Each type of battery chemistry boasts its own unique perks. For wearable electronics designers and engineers, this informative piece is meant to help in choosing the most fitting chemistries for affordable wearable applications of today, with a focus on designing that is straightforward [9,10]. These particular answers work nicely for applications with space restrictions and a need for thriftiness and can even speed up the marketing process [11,12]. Due to their environmental compatibility, extended lifetime, and high energy density, rechargeable lithium-ion batteries (LIB) have gained widespread use in an array of fields. These energy storage devices are quite versatile, servicing applications ranging from public utilities to consumer electronics to hybrid and electric vehicles [13,14].

Used widely in lithium-ion batteries, the cathode material known as layered LiCoO_2 offers both great cycle durability and convenience in production, thanks to its reliable discharge capacity [15]. A similarly popular cathode material, layered LiNiO_2 [16], has been noted for its more exacting production criteria [17]; therefore, a hybrid of the two known as $\text{LiNi}_{1-x}\text{Co}_x\text{O}_2$ has gained attention [18] for its ability to blend the best features of both LiNiO_2 and LiCoO_2 .

* Corresponding author: muhammادتimimi@yahoo.com

<https://doi.org/10.15251/JOR.2023.196.783>

2. Experimental part

Urea (based on the molecular formula $\text{NH}_2\text{CO.NH}_2$, with a mass of 60.06 g/mol), citric acid (mass of 192.13 g/mol), nitric acid (HNO_3 , 70%), along with lithium chloride (LiCl , MW = 42.39), cobalt(II) chloride hexahydrate ($\text{CoCl}_2\cdot 6\text{H}_2\text{O}$, MW = 237.93 g/mol), and nickel(II) chloride hexahydrate ($\text{NiCl}_2\cdot 6\text{H}_2\text{O}$, MW = 237.71 g/mol), are the raw materials required for producing NCM cathode materials using the urea route (urea sol-gel) through a process that involves stoichiometric amounts of lithium chloride (LiCl), cobalt (II) chloride ($\text{CoCl}_2\cdot 6\text{H}_2\text{O}$), and nickel (II) chloride ($\text{NiCl}_2\cdot 6\text{H}_2\text{O}$) as Li ion precursors. The process begins by completely dissolving these precursors in distilled water after which they should be mixed thoroughly while being stirred continuously. The molecular weight of the raw materials used is 63.01 g/mol. The first solution was constantly mixed and added with an aqueous solution composed of urea ($\text{NH}_2\text{CO.NH}_2$) and citric acid ($\text{C}_6\text{H}_8\text{O}_7$) to form a starting solution (100mL). To maintain a balance of metal ions, the molar ratio of citric acid to total metal ions was adjusted to 1:2, whereas the molar ratio of urea to total metal ions was adjusted to 1:1. Last but not least, under continuous stirring, nitric acid (HNO_3) was mixed in with the starting solution at a volumetric ratio of 1:0.1.

At intervals, the solution was stirred thoroughly and heated to 85°C for a duration of 4 hours to eliminate water. Gradually, the solution turned into a dark blue resin with occasional foaming while the viscosity increased. Eventually, a dark blue gel was achieved and the evaporation process was stopped. Next, the resin was placed in an oven and subjected to heat at 180°C for 6 hours until dried. Intermediate compounds called polymerization intermediates are formed as the gel volume undergoes a three to four times increase when compared to its initial size. Figure 1 (a, b, c, d, e) depicts the calcination process, which involved heating it at 800°C for 4 hours.

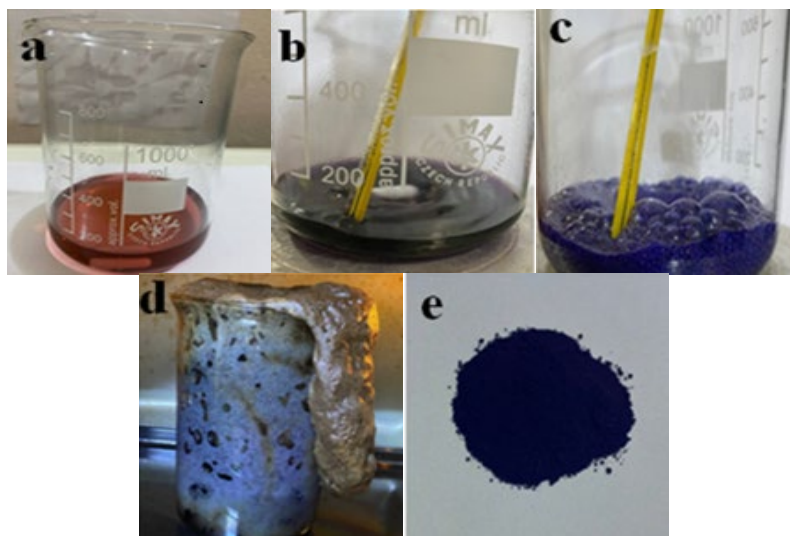


Fig. 1. The steps for the preparation process.

3. Results and discussion

3.1. X-ray Diffraction (XRD)

Using a Shimadzu XRD-6000 powder diffractometer and $\text{Cu-K}\alpha$ radiation, the structure type and crystal size of LiMO_2 ($\text{M}=\text{Co}, \text{Ni}$) nanopowder samples were analyzed through XRD testing. The prepared LiCoO_2 doped with varying proportions of Ni metal (0, 0.25, 0.5, 0.75 and 1 wt%) demonstrated characteristic peaks at $2\theta = 37.19^\circ, 38.86^\circ, 44.99^\circ, 59.28^\circ$ and 65.07° on the (101), (012), (104), (107) and (018) planes, respectively, indicating a hexagonal crystal system. The data matched closely with the standard (JCPDS 98-01-4801) for the LiCoO_2 space group nanostructure (R-3m No. 166), ($a=b=2.83 \text{ \AA}$, $c=14.119 \text{ \AA}$), ($\alpha=\beta=90^\circ$, $\gamma=120^\circ$). Additionally,

other peaks observed on the (022) and (224) planes at $2\Theta = 31.38^\circ$ and 55.86° , respectively, were attributed to the formation of cubic Co_3O_4 nanostructures of space group (Fd) - 3m No. 227), ($a=b=c= 8.0560 \text{ \AA}$), ($\alpha=\beta=\gamma= 90^\circ$), as shown in Figure 2.

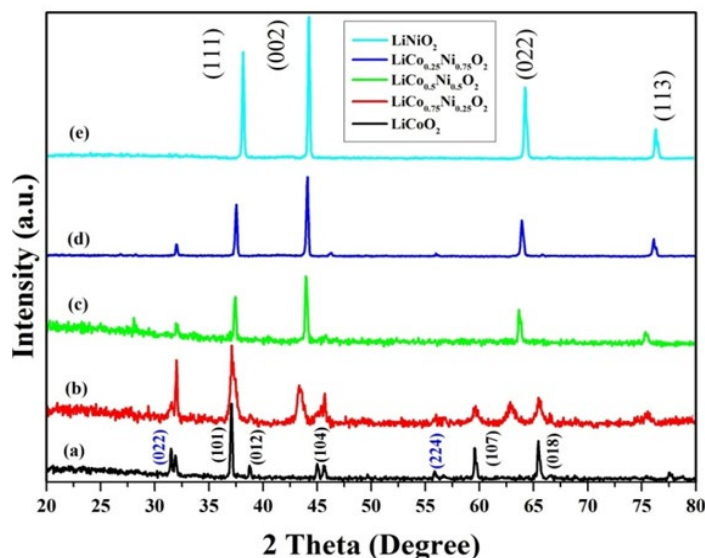


Fig. 2. XRD pattern of $(\text{LiCo}_{1-x}\text{Ni}_x\text{O}_2)$ sample.

As shown in Figure 2(b), the XRD pattern of the prepared LiCoO_2 doped with Ni metal ($x = 0.25$) shows that there are two new peaks at ($2\Theta = 43.96^\circ$ and 63.92°), which is due to the cubic caused by formation. Patterned LiCoO_2 nanostructures. As the Ni content increases (Co content decreases), these peaks shift slightly to the right from their original positions and become sharper with increasing intensity, confirming the successful integration of Ni ions into the LiCoO_2 lattice [17]. When the Ni content is $x=0.5$ and 0.75 , the cubic LiNiO_2 nanostructure phase becomes the main phase, as shown in Figure 2 (c, d). Figure 2(e) shows the XRD pattern of the prepared LiNiO_2 (Ni content $x=1$). The peaks detected at ($2\Theta = 37.82^\circ, 43.93^\circ, 63.92^\circ$ and 76.73°), corresponding to planes (111), (002), (022) and (113) respectively, towards the formation of pure compound cubic LiNiO_2 have Nanostructures of the space group (Fm-3m No. 225) where ($a = b = c = 4.1160 \text{ \AA}$) and ($\alpha = \beta = \gamma = 90^\circ$). These results were in good agreement with the standard data (JCPDS 98-002-9236) and no further impurity peaks were detected, confirming the high purity phase [18]. The crystal size of the prepared LiCoO_2 doped with different proportions of Ni metal (0, 0.25, 0.5, 0.75 and 1 wt%) was calculated using the highest peak intensity of the Debye-Scherrer equation. Sizes determined (40.15, 12.66, 31.54, 34.53, and 38.49 nm). Table 1 shows the XRD calculation results of the prepared samples. It was observed that the crystal size of the as-prepared LiCoO_2 nanostructures decreased when Ni metal was added, which was due to the suppression of crystal growth within the LiCoO_2 lattice by Ni ions. On the contrary, increasing Ni content leads to larger crystal size, which is consistent with previous studies [19, 20, 21].

Table 1. XRD calculations of prepared LiCoO_2 doped with different ratio of Ni.

Sample	2Θ (deg) Practical	2Θ (deg) Standard	FWHM (deg)	Crystalline size (nm)	d_{hkl} (\AA) Practical	d_{hkl} (\AA) Standard	(hkl)
LiCoO_2	37.19	37.2	0.18752	40.15	2.4156	2.4147	(101)
$\text{LiCo}_{0.75}\text{Ni}_{0.25}\text{O}_2$	37.22	37.2	0.59452	12.66	2.4137	2.4147	(101)
$\text{LiCo}_{0.5}\text{Ni}_{0.5}\text{O}_2$	43.78	43.96	0.23371	31.54	2.0561	2.0580	(002)
$\text{LiCo}_{0.25}\text{Ni}_{0.75}\text{O}_2$	43.85	43.96	0.21341	34.53	2.0571	2.0580	(002)
LiNiO_2	43.93	43.96	0.19141	38.49	2.0584	2.0580	(002)

3.2. Fourier Transform Infrared (FTIR)

In Fig. 3, the FTIR spectra of LiCoO_2 and $(\text{LiCo}_{1-x}\text{Ni}_x\text{O}_2)$ were analyzed within the 400-4000 cm^{-1} range. A wide-ranging band between 570 to 867 cm^{-1} was present in all samples, and it was identified as Bend and bend. Stretching vibrations of M-O and O-M-O bonds (where M = Li, Ni, and Co) [22,23]. Two bands were also observed in the 1315-1369 cm^{-1} and 1512-1516 cm^{-1} regions. These were identified as the asymmetric and symmetric vibrations of COO^- ions in metal carboxylates, respectively, confirming the chelation of metal ions by the FTIR spectrum. All of this culminates [24]. The C=O and O-C=O groups could be related to ketone formation, which might result from citric acid decomposition. This was indicated by the band observed near 1647–1739 cm^{-1} , corresponding to the carbonyl group. As for the broad band detected near 3421-3441 cm^{-1} , it's attributed to moisture absorption's O-H stretching vibration [26,27].

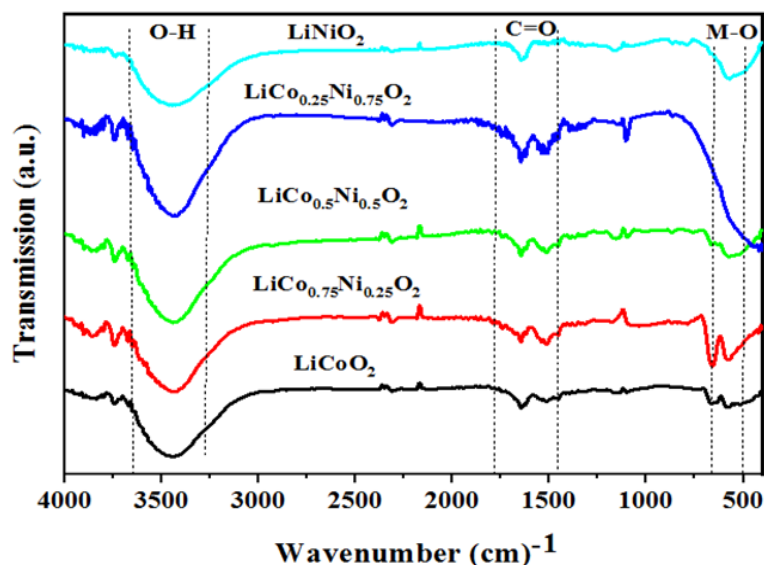


Fig. 3. FTIR spectra of $(\text{LiCo}_{1-x}\text{Ni}_x\text{O}_2)$ samples.

3.3. Field-Emission Scanning Electron Microscopy

Well-formed polycrystalline material comprising round polyhedral crystals was examined via FESEM analysis as shown in Figure 4. This examination was performed on LiCoO_2 and $(\text{LiCo}_{1-x}\text{Ni}_x\text{O}_2)$ powders ($x = 0, 0.25, 0.5, 0.75, 1$) that were prepared using the urea method. The FESEM images reveal that larger particles were formed as a result of crystals easily aggregating. Additionally, all of the samples showed positive results in terms of morphology. This information was compiled from [28,29]. The addition of Ni to the LiCoO_2 lattice seems to have an impact on the size of its crystallites, reducing them in the case of $(\text{LiCo}_{1-x}\text{Ni}_x\text{O}_2)$ material. Specifically, it appears that LiCoO_2 has a smaller crystal size when compared to materials that have been substituted with Ni [30,31].

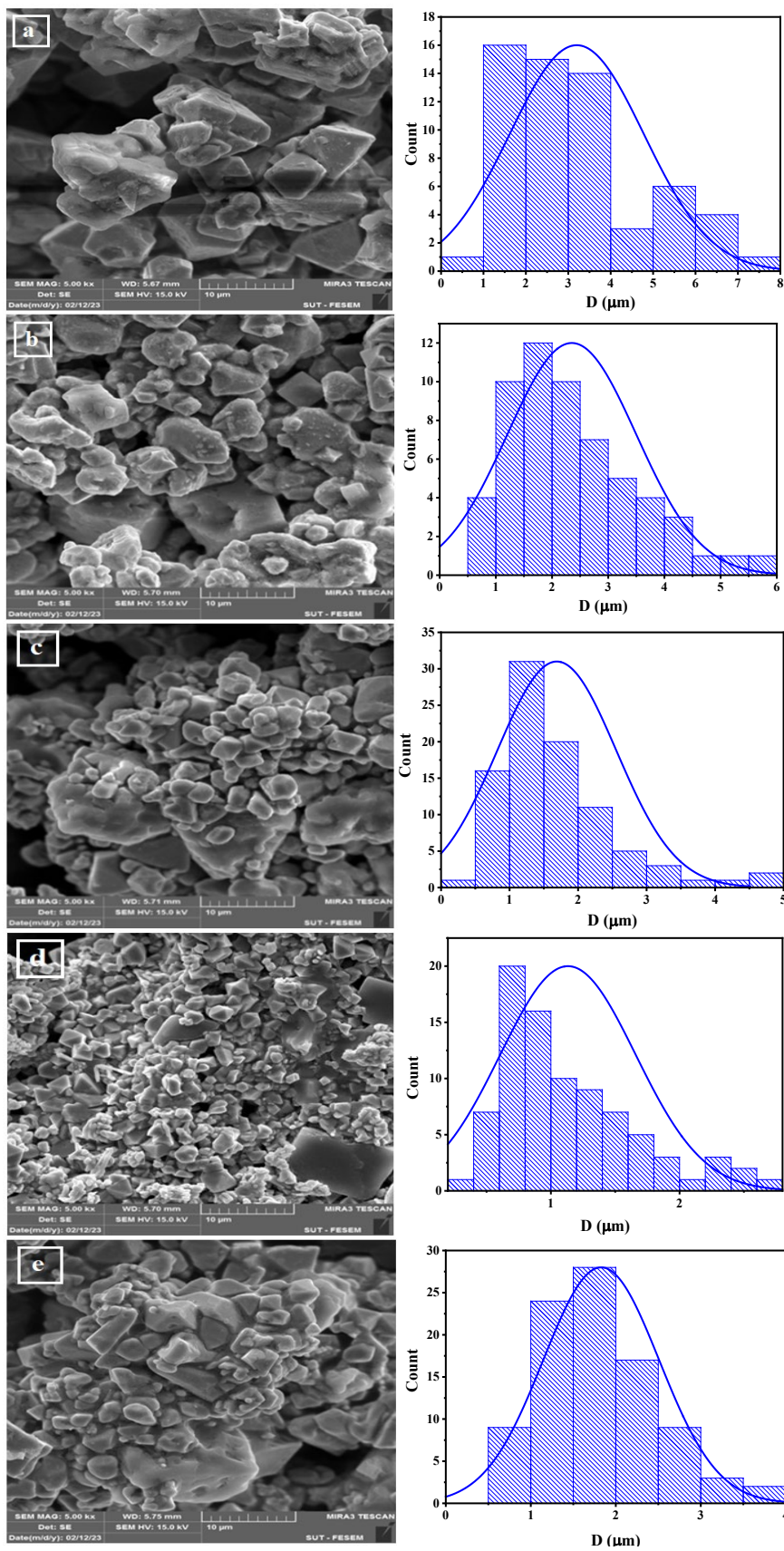


Fig. 4. FESEM images for : (a) LiCoO_2 , (b) $\text{LiCo}_{0.75}\text{Ni}_{0.25}\text{O}_2$, (c) $\text{LiCo}_{0.5}\text{Ni}_{0.5}\text{O}_2$, (d) $\text{LiCo}_{0.25}\text{Ni}_{0.75}\text{O}_2$, (e) LiNiO_2 .

3.4. X-ray energy dispersive spectroscopy (EDX)

Using energy-dispersive X-ray spectroscopy (EDX), the mixture's components and their percentages were determined. Table 2 displays figure 5(a)-(e), which reveals the weight percent of Co, Ni, O and C present in LiCoO_2 and $\text{LiCo}_{1-x}\text{Ni}_x\text{O}_2$ samples sintered at 800°C . The Li peak is not evident in figure 5(a)-(e), which is attributable to the ultrasoft nature of Li-K X-rays that have an energy level around 55 eV, causing low X-ray production and high absorption likelihood, leading to an extremely weak emitted signal [18].

Table 2. The (EDX) Ratios of the Elements of the ($\text{LiCo}_{1-x}\text{Ni}_x\text{O}_2$) samples.

Sample	Element	Weight %	Atomic %
LiCoO_2	Co	86.87	64.24
	O	13.13	35.76
	Total	100.00	100.00
$\text{LiCo}_{0.75}\text{Ni}_{0.25}\text{O}_2$	Co	64.01	45.83
	Ni	21.24	15.26
	O	14.76	38.91
	Total	100.00	100.00
$\text{LiCo}_{0.5}\text{Ni}_{0.5}\text{O}_2$	Co	42.11	30.55
	Ni	43.85	31.93
	O	14.04	37.52
	Total	100.00	100.00
$\text{LiCo}_{0.25}\text{Ni}_{0.75}\text{O}_2$	Co	22.58	16.55
	Ni	63.95	47.06
	O	13.47	36.38
	Total	100.00	100.00
LiNiO_2	Ni	62.39	62.39
	O	37.61	37.61
	Total	100.00	100.00

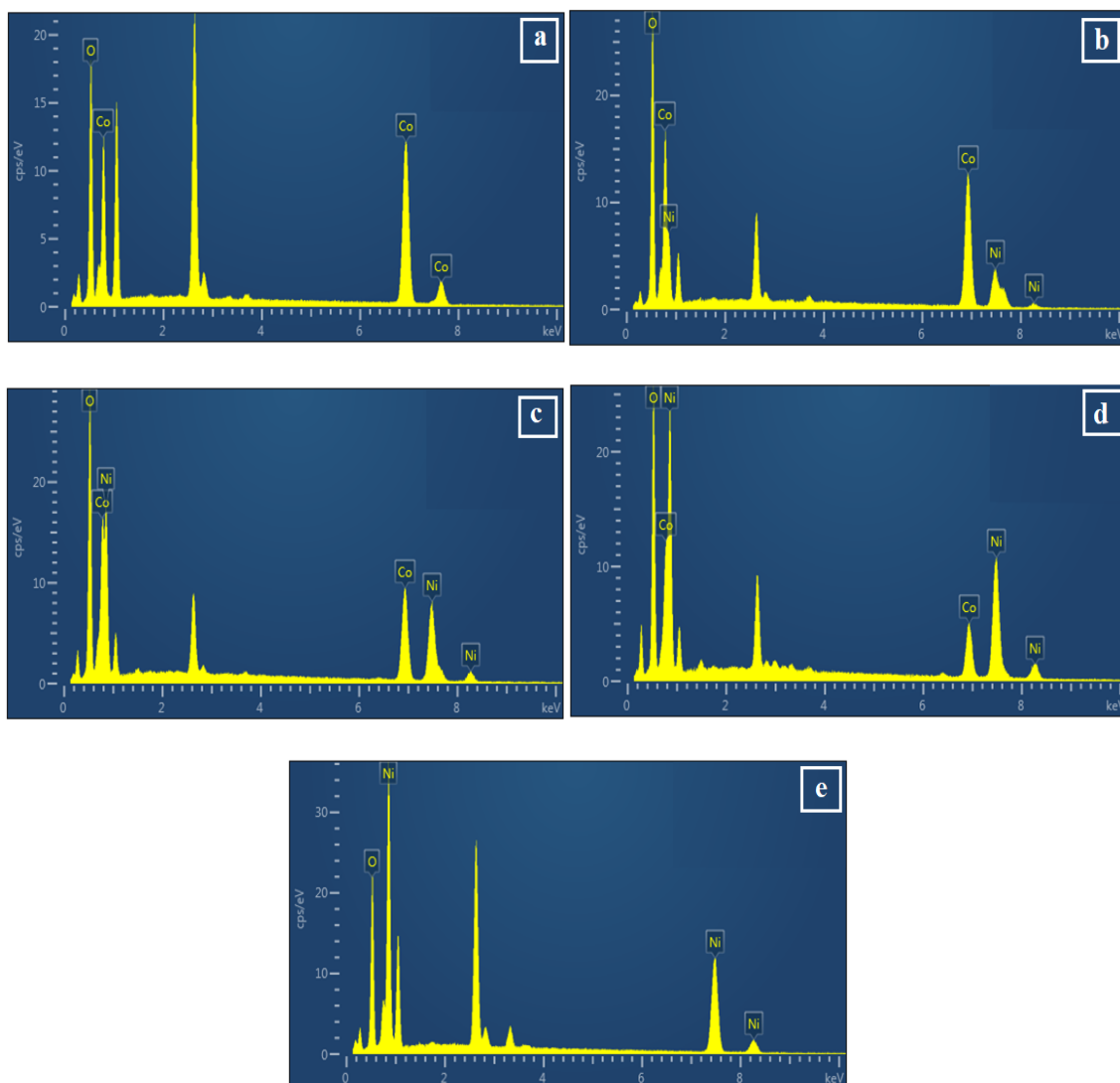


Fig. 5. EDX spectra for: (a) LiCoO_2 , (b) $\text{LiCo}_{0.75}\text{Ni}_{0.25}\text{O}_2$, (c) $\text{LiCo}_{0.5}\text{Ni}_{0.5}\text{O}_2$, (d) $\text{LiCo}_{0.25}\text{Ni}_{0.75}\text{O}_2$, (e) LiNiO_2 .

4. Conclusions

$\text{LiCo}_{1-x}\text{Ni}_x\text{O}_2$ nanoparticles were synthesized via the urea route and then calcined at 800°C for 4 hours. Structural characterization, especially X-ray diffraction (XRD), clearly confirmed the presence of second phases, including LiCoO_2 and Co_3O_4 phases. XRD analysis also provided evidence of successful incorporation of Ni ions into the LiCoO_2 lattice. Furthermore, the crystal size of the prepared LiCoO_2 nanostructures was reduced by adding Ni metal.

These nanoparticles have crystallite sizes in the nanometer range. FTIR analysis provides valuable information about the chemical bonds in a material, helping us understand its composition. FE-SEM analysis showed that all samples had nanostructural dimensions, while EDX confirmed the elemental composition of the synthesized materials. It is worth noting that the quantity and quality of additives play a crucial role in influencing all these factors. These findings significantly advance our understanding of the properties and potential applications of these materials in various fields, including energy storage and catalysis.

References

- [1] Kumar, U. P., Nesaraj, A. S. (2013), *J. Nano. Adv. Mat.*, 1(2), 75-86;
<https://doi.org/10.9734/AJOPACS/2017/34683>
- [2] Chu, B. (2007), *Energy*, 210(320), 160-230.
- [3] Luo, L., Tan, S. Y., Ma, C. (2021), *International Journal of Electrochemical Science*, 16(7), 210713; <https://doi.org/10.20964/2021.07.18>
- [4] Song, M., Kwon, I., Shim, S., Song, J. H. (2010), *Ceramics International*, 36(4), 1225-1231;
<https://doi.org/10.1016/j.ceramint.2010.01.008>
- [5] Song, M. Y., Lee, R. (2002), *Journal of power sources*, 111(1), 97-103;
[https://doi.org/10.1016/S0378-7753\(02\)00263-X](https://doi.org/10.1016/S0378-7753(02)00263-X)
- [6] Song, M., Kwon, I., Kim, H., Shim, S., Mumm, D. R. (2006), *Journal of applied electrochemistry*, 36, 801-805; <https://doi.org/10.1007/s10800-006-9138-7>
- [7] Abdullah, M. Z., Al-Timimi, M. H., Albanda, W. H., Dumitru, M., Balan, A. E., Ceaus, C., Stamatin, I. (2019), *Digest Journal of Nanomaterials and Biostructures*, 14(4), 1179-1193.
- [8] Abdullah, M. Z., Hasan, H. M., Al-Timimi, M. H., Albanda, W. H., Alhussainy, M. K., Dumitru, M. (2019), *Journal of Ovonic Research Vol*, 15(3), 199-204.
- [9] Sun, B. R., Zhou, A. G., Li, X., Yu, H. Z. (2021), *ACS sensors*, 6(5), 1731-1744;
<https://doi.org/10.1021/acssensors.1c00512>
- [10] Al-Mgrs, S. S. H., Al-Timimi, M. H., Abdullah, M. Z., Al-Banda, W. H. (2023, March), *AIP Conference Proceedings* (Vol. 2475, No. 1). AIP Publishing;
<https://doi.org/10.1063/5.0102768>
- [11] Saeed, F. R., Serban, E. C., Vasile, E., Al-Timimi, M. H. A. A., Al-Banda, W. H. A., Abdullah, M. Z. A., Balan, A. E. (2017), *Digest Journal of Nanomaterials and Biostructures*, 12(2), 273-280.
- [12] Mohammed, A. A., Ahmed, A. R., Al-Timimi, M. H. (2022), *Technium BioChemMed*, 3(2), 107-119; <https://doi.org/10.47577/biochemmed.v3i2.7116>
- [13] Saeed, F. R., Al-Timimi, M. H. A. A., Al-Banda, W. H. A., Abdullah, M. Z., Stamatin, I., Voinea, S., Balan, A. E. (2018), *Journal of Ovonic Research*, 14(5).
- [14] Al-Timimi, M. H., Albanda, W. H., Abdullah, M. Z. (2023), *East European Journal of Physics*, (2), 173-181; <https://doi.org/10.26565/2312-4334-2023-2-17>
- [15] Elong, K., Roshidah, R., Mohd Mokhtar, N. A., Azahidi, A., Kamarulzaman, N. (2012). *Advanced Materials Research*, 545, 182-184;
<https://doi.org/10.4028/www.scientific.net/AMR.545.182>
- [16] Chokshi, N. P., & Ruparelia, J. P. (2020), *Journal of The Institution of Engineers (India): Series A*, 101, 433-443; <https://doi.org/10.1007/s40030-020-00454-4>
- [17] Wang, Y., Cheng, T., Yu, Z. E., Lyu, Y., Guo, B. (2020), *Journal of Alloys and Compounds*, 842, 155827; <https://doi.org/10.1016/j.jallcom.2020.155827>
- [18] Nguyen, T. P., Giang, T. T., Kim, I. T. (2022), *Chemical Engineering Journal*, 437, 135292;
<https://doi.org/10.1016/j.cej.2022.135292>
- [19] Zhu, J., & Chen, G. (2019), *Journal of Materials Chemistry A*, 7(10), 5463-5474;
<https://doi.org/10.1039/C8TA10329A>
- [20] Li, Y., Jiang, H., Huang, W., Tian, H. (2008), *Applied Surface Science*, 254(21), 6865-6869;
<https://doi.org/10.1016/j.apsusc.2008.04.087>
- [21] Li, J., Li, H., Stone, W., Weber, R., Hy, S., Dahn, J. R. (2017), *Journal of The Electrochemical Society*, 164(14), A3529; <https://doi.org/10.1149/2.0401714jes>
- [22] Ayoub, R. H., AL-Timimi, M. H., Abdullah, M. Z. (2023), *East European Journal of Physics*, (3), 546-554; <https://doi.org/10.26565/2312-4334-2023-3-64>
- [23] Razzak, A. A., Al-Gebori, A. M., Haider, M. J. (2020), *Progress in Industrial Ecology, an International Journal*, 14(1), 19-29; <https://doi.org/10.1504/PIE.2020.105195>
- [24] Al-Mgrs, S. S. H., Al-Timimi, M. H., Abdullah, M. Z., Al-Banda, W. H. (2023, March), *AIP*

Conference Proceedings (Vol. 2475, No. 1). AIP Publishing; <https://doi.org/10.1063/5.0102768>

[25] Vivekanandhan, S., Venkateswarlu, M., Satyanarayana, N. (2008), Journal of alloys and compounds, 462(1-2), 328-334; <https://doi.org/10.1016/j.jallcom.2007.08.055>

[26] Gómez-Cuaspad, J. A., Neira-Guio, A. Y., Vera-López, E., Canaria-Camargo, L. C. (2020), Universitas Scientiarum, 25(2), 203-225; <https://doi.org/10.11144/Javeriana.SC25-2.csas>

[27] Hussein, H. M., & Al-Timimi, M. H. (2022), Eurasian Journal of Physics, Chemistry and Mathematics, 8, 47-55.

[28] Aelawi, W. A., Alptekin, S., Al-Timimi, M. H. (2023), Indian Journal of Physics, 1-8; <https://doi.org/10.1007/s12648-023-02736-6>

[29] Matus, M., Kamarulzaman, N., Mastuli, M. S., Abdillih, N. S. S. M., Elong, K. E. L. I. M. A. H. (2020), Solid State Phenomena, 307, 136-140; <https://doi.org/10.4028/www.scientific.net/SSP.307.136>

[30] Al-Rikabi, H. S., Al-Timimi, M. H., Abed, A. H., Albanda, W. (2022), Diyala Journal for Pure Science, 18(4); <https://doi.org/10.24237/djps.1804.607D>

[31] Mohd Abdillih, N. S. S., Kamarulzaman, N., Elong, K., & Mastuli, M. S. (2020), Solid State Phenomena, 307, 113-118; <https://doi.org/10.4028/www.scientific.net/SSP.307.113>